Materials Horizons

ROYAL SOCIETY OF CHEMISTRY

COMMUNICATION

View Article Online
View Journal | View Issue

Cite this: *Mater. Horiz.*, 2020, 7, 1171

Received 25th September 2019,
Accepted 7th January 2020

DOI: 10.1039/c9mh01524h

rsc.li/materials-horizons

Unveiling the underlying mechanism of record-high efficiency organic near-infrared photodetector harnessing a single-component photoactive layer†

Miaosheng Wang,[a] Ya-Ze Li,[b] Hung-Cheng Chen,[c] Che-Wei Liu,[b] Yi-Sheng Chen,[c] Yuan-Chih Lo,[c] Cheng-Si Tsao,[de] Yu-Ching Huang,[f] Shun-Wei Liu,*[bg] Ken-Tsung Wong*[ch] and Bin Hu*[a]

This paper demonstrates high-efficiency organic near-infrared (NIR) photodetection activity by increasing the symmetry of photoinduced charge density based on planar cyclic donor–acceptor structures. The record-high photosensing capability (gain: 3×10^5 and EQE: 43% at 3 V) is realized under NIR 780 nm illumination upon using the single-component active layer chloroaluminum phthalocyanine (ClAlPc) with planar cyclic intramolecular donor–acceptor structures to create four-fold symmetry of photoinduced charge density. Our *in situ* measurement using bias-dependent magneto-photocurrent reveals that increasing the symmetry of photoinduced charge density through planar cyclic intramolecular donor–acceptor structures can significantly decrease the electron–hole binding energies, allowing the direct generation of free photogenerated carriers without any heterojunction structures. Particularly, with the four-fold symmetry of photoinduced charge density, the dissociation of electron–hole pairs can be completed at an extremely low critical bias (24.8 mV) in the ClAlPc molecules. Such low critical bias provides the underlying mechanism to directly generate free carriers in the single-component active layer under NIR illumination. Clearly, by using planar cyclic intramolecular donor–acceptor structures, symmetrically arranging photoinduced charge density presents a fundamental strategy to develop high-efficiency NIR sensing capabilities with single-component active layer design in organic molecules.

New concepts

In this work, for the first time, by utilizing the four-fold symmetric **ClAlPc** molecules as the single-component active layer, we have successfully demonstrated a record-high efficiency near-infrared (NIR) thin-film organic photodetector (OPD) comparable with the commercial standard silicon photodetector (Si-PD). The **ClAlPc** OPD shows a record-high external quantum efficiency (EQE) value of 43% (at 3 V). Meanwhile, this **ClAlPc** OPD exhibits the largest linear dynamic range (LDR) of 170 dB with 8 orders of magnitude difference in photocurrent response as compared with all previously reported NIR OPDs. With the ultra-thin (10 nm) single-component active layer design, the **ClAlPc** OPD can realize a high response speed similar to Si-PD. The demonstration of this high-efficiency single-component active layer OPD indicates a new fundamental mechanism to directly generate free photocarriers without using heterojunctions in organic materials. By using the magneto-photocurrent as an *in situ* method to monitor the dissociation of photogenerated electron–hole pairs, we found that increasing the symmetry of charge density can significantly lower the electron–hole binding energy from eV to meV order. Clearly, increasing the symmetry of charge density through a planar conjugated macrocyclic design presents a new mechanism to significantly lower the electron–hole binding energy in organic materials towards thin-film energy-related optoelectronic applications.

Introduction

Organic photodetectors (OPDs) converting light energy into electric current are aiming for the precise detection of low-level photons. The absorption features of organic materials allow OPDs to perform with a wide spectral response together with low dark current density, high sensitivity, and reasonably fast response time, rendering this technology feasible for applications such as image sensors[1] and artificial vision.[2] Particularly interesting, near-infrared (NIR)-responsive OPDs are emerging

[a] *Department of Materials Science and Engineering, University of Tennessee, Knoxville, TN 37996, USA. E-mail: bhu@utk.edu*
[b] *Department of Electronic Engineering, Ming Chi University of Technology, New Taipei City 24301, Taiwan. E-mail: swliu@mail.mcut.edu.tw*
[c] *Department of Chemistry, National Taiwan University, Taipei 10617, Taiwan. E-mail: kenwong@ntu.edu.tw*
[d] *Department of Materials Science and Engineering, National Taiwan University, Taipei 106, Taiwan*
[e] *Institute of Nuclear Energy Research, Taoyuan 325, Taiwan*
[f] *Department of Materials Engineering, Ming Chi University of Technology, New Taipei City 24301, Taiwan*
[g] *Organic Electronics Research Center, Ming Chi University of Technology, New Taipei City 24301, Taiwan*
[h] *Institute of Atomic and Molecular Science, Academia Sinica, Taipei 10617, Taiwan*
† Electronic supplementary information (ESI) available. See DOI: 10.1039/c9mh01524h

candidates for biomedical diagnosis[3] and health sensors,[4] in addition to optical communication[5] and night vision[6] applications. In order to have organic materials with NIR-responsive character, the most feasible strategy is to utilize fully conjugated donor–acceptor-type polymers as the donors in conjunction with fullerene derivatives as acceptors for OPDs. For example, an OPD device employing a benzodithiophene and dithiadiazolo[3,4-*f*]-benzotriazole hybridized conjugated polymer (PTZBTTT-BDT) blended with $PC_{61}BM$ as the active layer contacted with a cross-linkable fluorene-based polymer (PFN-OX) as electron extraction layer delivered an external quantum efficiency (EQE) of 18.2% at 800 nm.[7] The EQE at 800 nm has been improved to *ca.* 30% by utilizing a polymeric donor PBD(EDOT) composed of thiophene-linked benzodithiophene and diketopyrrolopyrrole and the acceptor $PC_{61}BM$.[8] In addition to polymeric donors, solution-processed OPDs based on small-molecule donors also demonstrated good performance, for example, an OPD using a donor–acceptor porphyrin derivative (DHTBTEZP) as donor and $PC_{61}BM$ as acceptor can give an EQE of 23.5% at 800 nm.[9] The detection range can further extend to 850 nm with an EQE of 17.0% by introducing a cyanine dye Cy7-T as the NIR-responsive material together with a photo-polymerized C_{60} as acceptor. Interestingly, this cyanine dye-based OPD revealed a transparent character.[10] It is obvious that the fully conjugated polymer, as well as small-molecule donors, can exhibit efficient NIR absorption, and together with the good electron-transporting character of $PC_{61}BM$, renders the resultant OPDs with good EQEs in NIR region and low dark current for good sensitivity. However, there are some challenging issues on the lifespan of OPDs fabricated with solution processing techniques. One feasible solution for providing OPDs with comparable efficiency to those of solution-processed counterparts but with better lifetime performance is to use the well-established vacuum process compatible to the current OLED display technology. Unfortunately, small-molecule donors that simultaneously fulfill the NIR absorption and thermal stability requirements for vacuum deposition are very limited. Among the reported vacuum-processed NIR OPDs, those employing lead phthalocyanine (PbPc) as donor combined with pristine C_{60} as acceptor are the most successful cases. Even with vacuum deposition, there is still some room for device engineering, for example, a bilayer-type ($PbPc/C_{60}$) photoactive configuration has been demonstrated to give an EQE of 18.0% at 900 nm.[11] The efficiency can be further improved to 30.2% at 890 nm with planar-mixed bulk heterojunction (BHJ) configuration, where the photoresponsive $PbPc(5\%):C_{70}$ blend is sandwiched between a thin layer of PbPc and C_{70} for better exciton generation as well as electron/hole extraction.[12] In addition, control of the crystallinity of PbPc has been revealed not only to extend the response region to longer wavelengths but also to enhance the EQE up to 31.1% at 970 nm and a reverse bias of −3 V.[13] In spite of their advantage for efficiently catching photons, organic materials typically possess high electron–hole (exciton) binding energies due to low dielectric constants.[14,15] As consequence, for most organic NIR OPDs with high photogeneration yield, the photoresponsive layer is either a donor/acceptor bilayer-type or a donor:acceptor (D:A) blend (namely, a BHJ), not only for facilitating the charge carrier generation by virtue of photoinduced charge separation, but also for effective charge transport and collection.[16] Therefore, both the molecular design and device fabrication are crucial for manipulating the intermixed D:A morphologies. One feasible way to reduce the complexity of making efficient OPDs is to use a single component as the active layer. In this regard, there are still limited cases being reported to perform with promising efficiency due to the inferior photogeneration yield of photoactive materials.[17,18] Recently, the direct generation of free carriers by photoexcitation has been observed in some phthalocyanine-type molecules such as zinc phthalocyanine (ZnPc), boron subphthalocyanine chloride (**SubPc**), and boron subnaphthalocyanine chloride (SubNc) through spectroscopic measurements.[19–21] The observed direct generation of free carriers in single-component active layers under photoexcitation presents interesting evidence that these organic molecules possess extremely low electron–hole binding energies even with low dielectric constants. Fundamentally, this imposes a critical question on the underlying mechanisms that are accountable for the significantly low electron–hole binding energies in these organic materials. Technically, these results trigger a new possibility for exploring phthalocyanine-based materials as a single-component active layer to realize efficient OPDs without using BHJ designs.

In this work, for the first time, we demonstrate a high-efficiency NIR OPD by adopting the single-component active layer (phthalocyanine, **ClAlPc**) with four-fold symmetry of photoinduced charge density through planar cyclic intramolecular donor–acceptor structures. With photoexcitation at 780 nm, under a forward bias of 3 V, the device delivered an EQE reaching a record-high value of 43% and photocurrent gain ratio higher than 3×10^5. The outstanding performance of this single-component-based OPD implies that the **ClAlPc** thin film exhibits an extremely low electron–hole binding energy. This result stimulated our efforts to explore the underlying mechanisms responsible for such low electron–hole binding energy when the symmetry of photoinduced charge density exists through planar cyclic intramolecular donor–acceptor structures. By using *in situ* bias-dependent magneto-photocurrent measurement, the observed critical bias required to complete the dissociation of the electron–hole pairs in four-fold symmetric **ClAlPc** is extremely low (24.8 mV). The same protocol was also employed to examine other phthalocyanine derivatives, namely, three-fold symmetry **SubPc** and asymmetrical **ClAlNPc**. The observed critical bias largely increases to 128 mV for **SubPc** and 525 mV for **ClAlNPc**. Based on these results, we propose that the arrangement of photo-induced electric dipoles ($phenylene^{\delta+}$–$pyrrole^{\delta-}$) within planar cyclic intramolecular donor–acceptor structures is a crucial parameter to significantly lower the electron–hole binding energies in organic materials towards developing high-efficiency NIR OPDs by using a single-component active layer design.

Results and discussion

The device architecture of the single-component active layer NIR OPD was configured as ITO/**ClAlPc** (10 nm)/TAPC (90 nm)/MoO_3 (15 nm)/Al (120 nm) (Fig. 1a). The **ClAlPc** thin film functions as

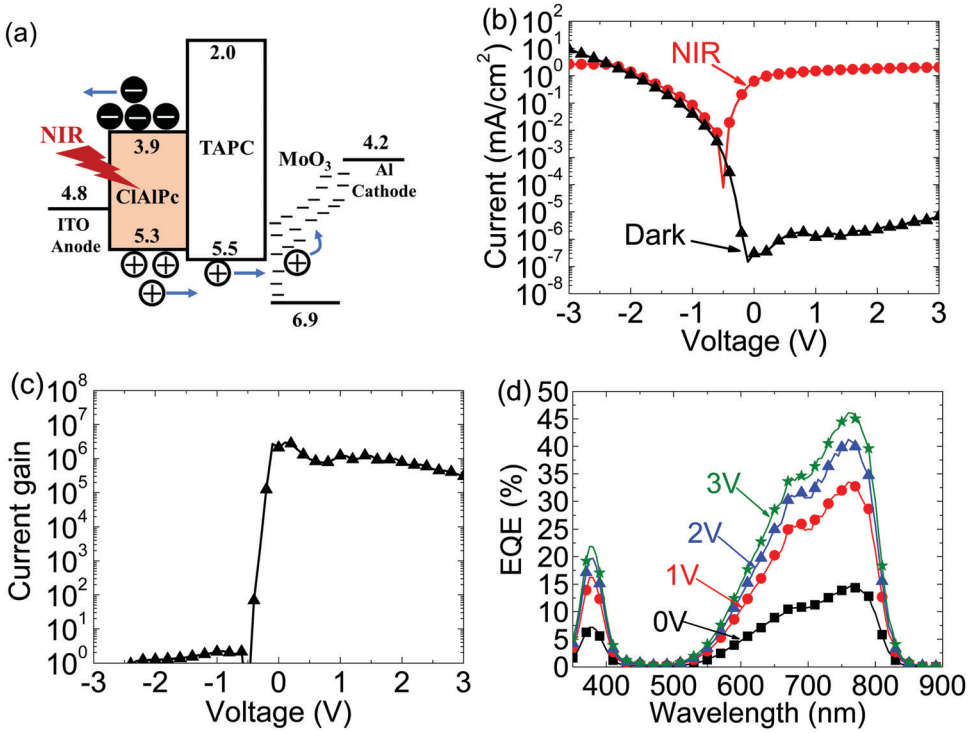

Fig. 1 Photodetector device performance characterization. (a) Energy-level diagram for the photodetector with **ClAlPc** as charge generation layer. The device structure is ITO/**ClAlPc** (10 nm)/TAPC (90 nm)/MoO_3 (15 nm)/Al (120 nm). (b) *I*–*V* curves under dark and NIR conditions for the **ClAlPc**-based photodetector. The NIR photoexcitation was provided by a 780 nm NIR LED with the intensity of 2 mW cm^{-2}. (c) Current gain, defined as the photocurrent divided by dark current, is shown as a function of bias. (d) EQE spectra under various biases.

an active layer to directly generate free carriers under NIR photoexcitation. The TAPC/MoO_3 acts as the hole transport layer. Under forward bias (>0 V), we defined the ITO and Al serving as anode and cathode, respectively. Therefore, the holes (electrons) come from the ITO (Al) electrode. In this situation, the holes and electrons are blocked at the ITO/**ClAlPc** and TAPC/MoO_3 interfaces, respectively, due to the potential barriers formed between the HOMO level of ITO (4.8 eV) and **ClAlPc** (5.3 eV), and the LUMO level of TAPC (2.0 eV) and the work function of MoO_3 (6.9 eV), respectively, leading to the ultralow current density reaching 1.2 nA cm^{-2} at an operating forward bias of 1.0 V under dark condition (Fig. 1b). Under the 2 mW cm^{-2} photoexcitation from a NIR LED at 780 nm, the photocurrent significantly increases, indicating the efficient generation of free charge carriers in the **ClAlPc** layer in the absence of BHJ structures. Specifically, the photocurrent gain ratio (defined as the photocurrent divided by dark current[22–24]) reaches 3×10^5 at a driving voltage of 3 V (Fig. 1c), while the EQE at 780 nm becomes 14% at zero bias and 43% at 3 V (Fig. 1d). Fig. S1 (ESI†) shows the EQE of the optimized thickness of 10 nm, 20 nm and 30 nm for the **ClAlPc** single-layer devices. The EQE decreases obviously with increasing **ClAlPc** thickness. In addition to the high EQE and photocurrent gain, the detectivity is another important parameter for evaluating the performance of a photodetector. Here, the specific detectivity was expressed as:

$$D^* = \frac{R}{\sqrt{2qJ_d}},$$

where R is responsivity (A W^{-1}), q is an elementary charge (1.6×10^{-19} Coulomb), and J_d is the dark current density (A cm^{-2}). At the operating wavelength of 780 nm and a bias of 3 V, the specific detectivity (D^*) reaches 5.8×10^{12} Jones based on our single-component active layer design (Fig. S2, ESI†), which is the highest among detectivity values of previously reported NIR OPDs prepared by multiple-component active layer architectures. To understand the correlation between the photocurrent and incident light intensity, we analyzed the linear dynamic range (LDR) of a commercial standard silicon-based photodetector (Si-PD, Newport 818-UV) to verify our measurement. As shown in Fig. 2a, the LDR of Si-PD under a bias of −0.5 V is as high as 230.6 dB with 11 orders of magnitude difference in photocurrent response to light power density, from 3.78 pW cm^{-2} to 1 W cm^{-2}. For our single-component **ClAlPc**-based OPD, under a bias of 0.5 V, the photocurrent linearly increases from 0.521 nA cm^{-2} to 0.163 A cm^{-2}, corresponding to light power density from 2.93 pW cm^{-2} to 1 W cm^{-2}, leading to an LDR of 170 dB with 8 orders of magnitude difference in photocurrent response. To our best knowledge, the LDR of our single-component **ClAlPc**-based OPD is the highest ever reported among NIR-responsive OPDs and comparable to the LDRs (160–200) reported in perovskite-based photoreactors.[25–28] It is noteworthy that the low dark current is revealed as the major factor responsible for the LDR difference between Si-PD and **ClAlPc**-based OPD. The defective interfacial contact between ITO and organic thin film is generally believed to lead to the higher leakage current of OPD.[29,30] In addition to LDR, the response speed of an OPD is also a crucial parameter, particularly important

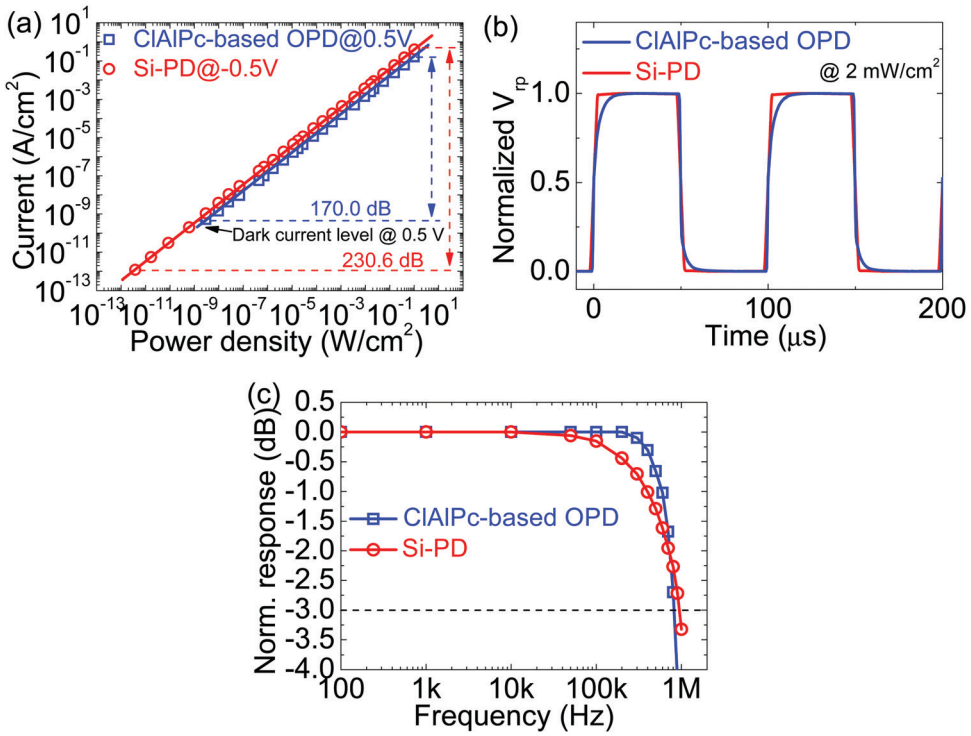

Fig. 2 (a) The comparison on linear dynamic range (LDR) for the **ClAlPc**-based OPD and commercial Si-PD (Newport 818-UV photodetector). The solid lines are the linear fitting. (b) Photocurrent response of **ClAlPc**-based OPD and the standard silicon PD to a 10 kHz light pulse at 780 nm with an incident power density of 2 mW cm^{-2}. (c) The cut-off frequency (f_{-3dB}) in Hz at reverse bias (3 V for **ClAlPc**-based OPD; −1 V for Si-PD).

for optical communication applications.[31–33] Fig. 2b shows the photocurrent responses of Si-PD and **ClAlPc**-based OPD under 10 kHz light pulse (780 nm) with an incident power density of 2 mW cm^{-2}. Accordingly, the rise/fall time can be extracted as 0.75/0.7 μs and 0.57/0.64 μs for the **ClAlPc**-based OPD and Si-PD, respectively. This result indicates that the response speed of our **ClAlPc**-based single-component OPD is comparable with the commercial standard Si-PD under the same conditions. Meanwhile, the charge-carrier mobility of **ClAlPc** was analyzed using the space charge-limited current (SCLC) method[34,35] by using a hole-only device configured as ITO/MoO_3 (10 nm)/**ClAlPc** (100 nm)/MoO_3 (10 nm)/Ag (120 nm). As shown in Fig. S3 (ESI†), the hole mobility of **ClAlPc** with the average value of 8.42×10^{-5} cm^2 V^{-1} s^{-1} was obtained in the applied electric fields (800–1000 V cm^{-1}). Noteworthy, although the charge mobility of **ClAlPc** is significantly lower (4–6 orders of magnitude) than that of p-Si, these two photodetectors still show similar response speeds. This result can be attributed to the direct generation of free carriers in the single-active layer (**ClAlPc**) that allows the use of an ultra-thin (10 nm) device structure. The dynamic response of Si-PD and **ClAlPc**-based OPD was measured with response frequency from 100 to 1 MHz under 780 nm light source with an incident power density of 2 mW cm^{-2}. As shown in Fig. 2c, the cut-off frequencies of **ClAlPc**-based OPD and Si-PD are 823.8 and 932.3 kHz at −3 dB, respectively, agreeing with the observed results shown in Fig. 2b. Moreover, the aging study showed stable light and dark current densities of the **ClAlPc**-based OPD with continuous light exposure (at 2 mW cm^{-2} 780 nm LED) and 3 V bias, indicating a decent stability for NIR sensing (Fig. S4, ESI†).

Clearly, the high NIR photosensing capability in the **ClAlPc**-based single-component active layer NIR OPD indicates the photogenerated electron–hole pairs can be efficiently dissociated into free charge carriers even without using any BHJ design. Here, we notice that the **ClAlPc** molecule consists of four planar isoindole rings symmetrically arranged into a planar cyclic structure with one vertical electric dipole ($Cl^{\delta-}$–$Al^{\delta+}$), as shown in Fig. 3a. By arranging four isoindole units with four-fold symmetry in a molecular ring, upon photoexcitation, the intramolecular charge transfer can lead to symmetrically arranged photoinduced electrical dipoles (phenylene$^{\delta+}$–pyrrole$^{\delta-}$) within a molecular ring. Due to the molecular symmetry, these four electrical dipoles (phenylene$^{\delta+}$–pyrrole$^{\delta-}$) encounter symmetrical head-to-head repulsive interactions, consequently decreasing the coulombic attraction within each electrical dipole. Essentially, this can significantly lower the electron–hole binding energy of **ClAlPc**. This presents a fundamental principle that introducing the symmetry of photoinduced charge density leads to a large reduction of electron–hole binding energy in organic molecules, known as low-dielectric materials. Here, we directly monitor the dissociation of electron–hole pairs in **ClAlPc** thin film by using bias-dependent magneto-photocurrent. Generally, the presence of magneto-photocurrent in organic semiconductors indicates that the electron–hole pairs are formed with singlet and triplet states under photoexcitation for the generation of photocurrent.[36] A magnetic field can change the populations on singlet and triplet electron–hole pairs by perturbing intersystem crossing, leading to the change in photocurrent,

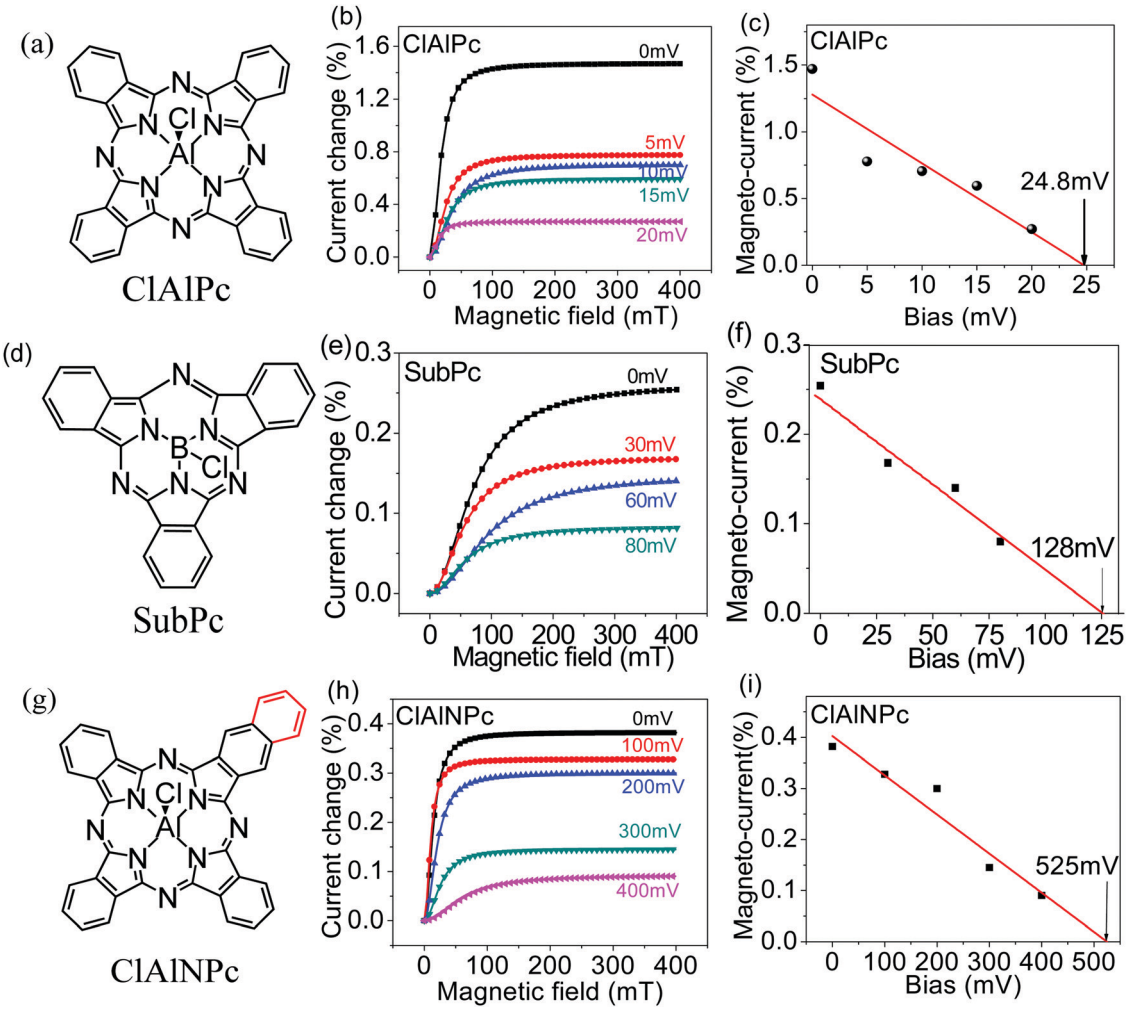

Fig. 3 Bias-dependent magneto-photocurrent for **ClAlPc** and **ClAlNPc**. (a) Chemical structure of the **ClAlPc** molecule. (b) Bias-dependent magneto-photocurrent and (c) magneto-photocurrent as a function of applied reverse bias for single-layer **ClAlPc** device (ITO/**ClAlPc** 50 nm/Al). (d) Chemical structure of the **SubPc** molecule. (e) Bias-dependent magneto-photocurrent and (f) maximum magnitude of the magneto-photocurrent as a function of applied reverse bias for the single-layer device (ITO/**SubPc** (50 nm)/Al). (g) Chemical structure of the **ClAlNPc** molecule. (h) Bias-dependent magneto-photocurrent and (i) magneto-photocurrent as a function of applied reverse bias for the single-layer **ClAlNPc** device (ITO/**ClAlNPc** (50 nm)/Al).

generating a magneto-photocurrent due to the different dissociation rates associated with singlets and triplets.[37] On the other hand, applying an external bias can increase the dissociation of electron–hole pairs,[38,39] decreasing magneto-photocurrent signal. When an external bias reaches a critical value, the magneto-photocurrent signal can be completely quenched. Essentially, this critical bias, required to completely quench the magneto-photocurrent signal, reflects the electron–hole binding energy. Therefore, combining the magneto-photocurrent with external bias provides a convenient experimental tool to *in situ* monitor the dissociation of electron–hole pairs in organic materials when an external bias is applied.[40,41] Fig. 3b shows the bias-dependent magneto-photocurrent signal in the **ClAlPc** single-layer device with the structure of ITO/**ClAlPc** (50 nm)/Al. We can see that the photocurrent gradually increases and then becomes saturated with increasing magnetic field, leading to a magneto-photocurrent signal. More importantly, the magnitude of magneto-photocurrent signal is gradually decreased with increasing bias. This indicates that magneto-photocurrent can indeed reflect the dissociation of electron–hole pairs generated in the **ClAlPc** film with gradually increasing bias imposed on the ITO/**ClAlPc**/Al device. By plotting magneto-photocurrent amplitude against bias (Fig. 3c), we can determine that the electron–hole pairs are completely dissociated at the low bias of 24.8 mV, indicating the extremely small binding energy of electron–hole pairs, which is responsible for the efficient free charge carrier generation in **ClAlPc** molecule. This experimental result brings about a critical question on why free photogenerated carriers can be directly generated in organic materials which normally possess high electron–hole binding energies due to low dielectric constants.

To verify the symmetry-dependent electron–hole binding energies, we selected organic molecules (**SubPc** and **ClAlNPc**) with reduced symmetry of charge density. It is noticed that **SubPc** has been reported to exhibit direct free charge carrier generation under photoexcitation with a notable power conversion efficiency (PCE) of 0.3% in a single-layer device (ITO/**SubPc**/Al).[20] The **SubPc**

consists of three pyrrole–phenylene (isoindole) moieties with a permanent electric dipole of B^{+}–Cl^{-} (Fig. 3d). Clearly, the **SubPc** molecule possesses the three-fold symmetrical arrangement of electrical dipoles (phenylene$^{\delta+}$–pyrrole$^{\delta-}$), leading to three-fold symmetry of charge density. This three-fold symmetric **SubPc** should exhibit a weaker mutually repulsive interaction as compared with the four-fold symmetric **ClAlPc** molecule. Indeed, the critical bias required to completely dissociate electron–hole pairs of the **SubPc** thin film was determined by bias-dependent magneto-photocurrent to be 128 mV, indicating a larger binding energy as compared to that of **ClAlPc** film (Fig. 3e and f). To further investigate our hypothesis, we employed the same protocol on an asymmetric planar macrocyclic molecule **ClAlNPc** (Fig. 3g) with a structure fused with three pyrrole–phenylene (isoindole) moieties and one pyrrole–naphthylene structure (benzoisoindole). By breaking the symmetry of charge density, the dissociation of electron–hole pairs can become much more difficult, shown as a much higher bias to quench the magneto-photocurrent, as indicated by Fig. 3h. Thus, completely quenching the magneto-photocurrent requires a bias as high as 525 mV in the device with **ClAlNPc** thin film, where the symmetry of charge density is removed, as shown in Fig. 3i. This result indicates that perturbing the symmetry of charge density in a planar macrocyclic system causes a large increase in electron–hole binding energy. Clearly, increasing the symmetry of charge density presents an important mechanism to lower the electron–hole binding energy in organic macrocyclic molecules typically known as low-dielectric materials. Especially, the extremely low binding energy in the four-fold symmetric **ClAlPc** molecule significantly facilitates the photogeneration of free carriers in a photodetector with a single-component active layer, to realize the extraordinary NIR photosensing capability. To further explore the application of **ClAlPc** thin film as a single-component active layer, an ultimate solar cell configured as a single-layer device (ITO/**ClAlPc**/Al) was examined. This simple device can demonstrate a record-high PCE of up to 0.45% with V_{oc} of 0.76 V and J_{sc} of 1.3 mA cm^{-2} due to the extremely low binding energy (Fig. S5 and Table S1, ESI†) as compared with all other single-layer organic solar cells.[20] Here, we should point out that molecular packing is not an underlying factor in determining the electron–hole binding energy in **ClAlPc** films, based on the following two experimental indications. First, our magneto-photocurrent that was used to determine the electron–hole binding energy is a common phenomenon resulting from intramolecular electron-donating and electron-accepting structures. Second, our grazing-incidence wide-angle X-ray scattering (GIWAXS) and grazing-incidence small-angle X-ray scattering (GISAXS) studies have shown that the **ClAlPc** films contain crystalline nanograins and amorphous parts, as indicated in ESI† (Section IV). More importantly, such amorphous regions in the vertical direction increase with increasing film thickness (*e.g.* 50 nm), where the record-high PCE was realized in single-layer **ClAlPc** device configured as ITO/**ClAlPc** (50 nm)/Al. Clearly, our bias-dependent magneto-photocurrent measurements provide direct evidence that indicates the electron–hole binding energy is significantly lowered by increasing the symmetry of optically generated electrical dipoles within planar macromolecular structures. Overall, these results provide the precondition to further advance organic optoelectronics with a single-component active layer design.

Now we discuss the underlying mechanism responsible for the extremely low electron–hole binding energy. The **ClAlPc** molecule consists of four symmetrically arranged isoindole rings linked by four nitrogen bridges into a fully conjugated symmetric planar molecular ring with a vertical electric dipole ($Cl^{\delta-}$–$Al^{\delta+}$). Fig. 4 shows the electrostatic potential analysis of **ClAlPc** in excited states. It clearly indicates the charge density is symmetrically distributed on macrocycle. We should note that photoinduced charge transfer occurring at the isoindole moiety from the outer phenylene to inner pyrrole leads to optically generated electric dipoles (phenylene$^{\delta+}$–pyrrole$^{\delta-}$). With the four-fold symmetry of charge density, the four optically generated electric dipoles are symmetrically arranged with head-to-head configuration. Essentially, these symmetrically arranged optically generated electric dipoles with head-to-head configuration can decrease the attractive interaction between phenylene$^{\delta+}$ and pyrrole$^{\delta-}$ within each dipole, serving as the requirement to significantly lower the binding energy of photogenerated electron–hole pairs towards direct generation of photogenerated carriers. We should point out that this vertical dipole ($Cl^{\delta-}$–$Al^{\delta+}$) can significantly stabilize the formation of optically generated dipoles (phenylene$^{\delta+}$–pyrrole$^{\delta-}$) with four-fold symmetry in **ClAlPc** molecules. Without this vertical dipole, optically excited electrons in the inner ring have the possibility to quickly relax back to the

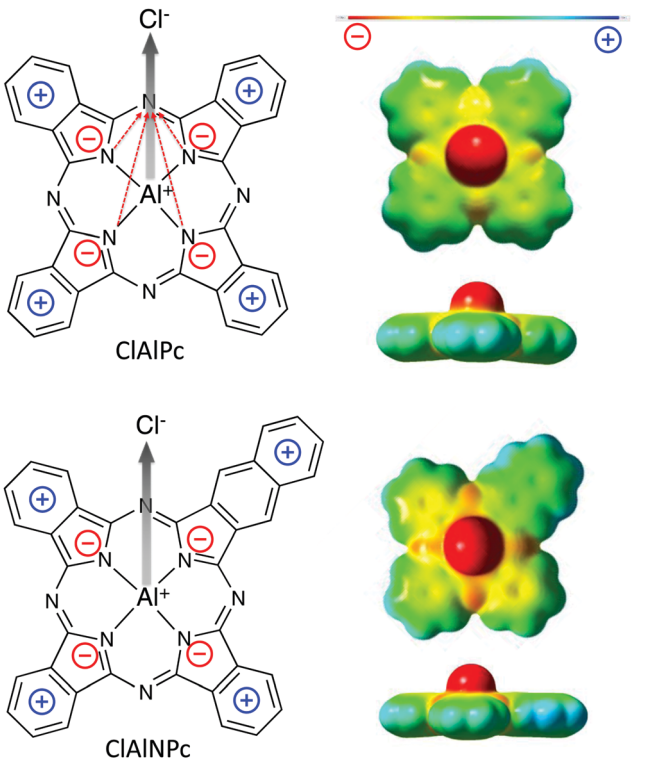

Fig. 4 Symmetrically arranged four isoindole rings of **ClAlPc** with a vertical electric dipole ($Cl^{\delta-}$–$Al^{\delta+}$) and asymmetrically arranged three isoindole rings and one benzoisoindole of **ClAlNPc** structure with a vertical electric dipole ($Cl^{\delta-}$–$Al^{\delta+}$), along with the calculated excited-state electrostatic potential maps of **ClAlPc** and **ClAlNPc**.

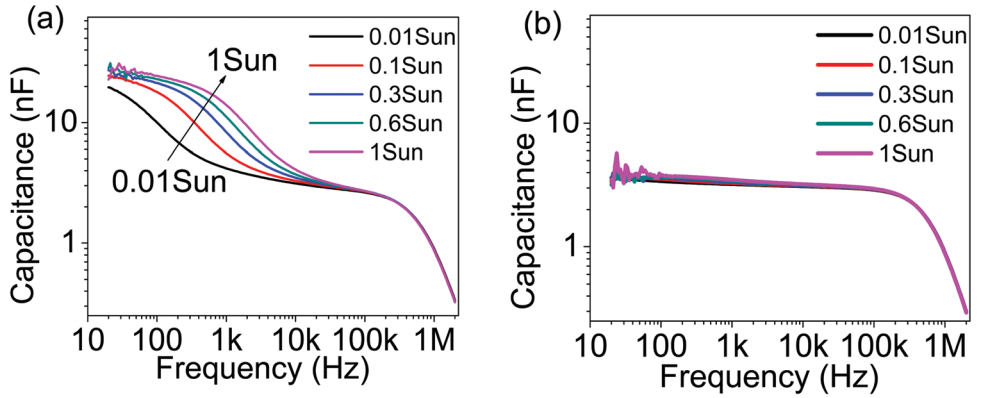

Fig. 5 *C–f* curves under simulated sunlight with variable intensities. (a) **ClAlPc** device (ITO/**ClAlPc** (50 nm)/Al). (b) **ClAlNPc** device (ITO/**ClAlNPc** (50 nm)/Al).

outer ring. Therefore, it is essential that the lifetime of optically generated dipoles must be sufficiently longer than the dissociation time of electron–hole pairs to demonstrate significantly reduced electron–hole binding energy. To verify our scenario, the parent phthalocyanine (Pc) without the electric dipoles (phenylene$^{\delta+}$–pyrrole$^{\delta-}$) was investigated (Fig. S6a, ESI†). The absorption coefficient of Pc is similar to those of **ClAlNPc** and **ClAlPc** molecules. It is interesting to note that it requires an extremely large bias of up to 2.35 V to completely quench the magneto-photocurrent signal (Fig. S6b and c, ESI†), indicating high electron–hole binding energy in the Pc molecule. In addition, the corresponding single layer-based device (ITO/Pc/Al) delivered a negligible photovoltaic effect with a PCE less than 0.01% (Fig. S6d, ESI†). Clearly, the vertical electric dipole plays an important role in realizing the low binding energy through head-to-head interaction under symmetric charge density.

To verify the formation of optically generated electrical dipoles through photoinduced charge transfer, the capacitance-frequency characteristics were examined for **ClAlPc** at different photoexcitation intensities (Fig. 5a). We can see that the photoexcitation clearly increases the signal amplitude around 1 kHz in the capacitance–frequency (*C–f*) curves of the **ClAlPc** molecule, while the **ClAlNPc** molecule shows a negligible change upon applying photoexcitation (Fig. 5b). The photoexcitation-dependent *C–f* characteristics provide evidence supporting that the electron withdrawing (pyrrole) and donating (phenylene) units, respectively, become negatively and positively charged within the **ClAlPc** molecule as a consequence of exciton dissociation due to extremely low electron–hole binding energy. In contrast, the photoinduced *C–f* curve (Fig. S6e, ESI†) of the Pc molecule shows an obvious enhancement at low frequency (less than 1 k Hz), indicating surface charge accumulation due to the insufficient charge transport without a permanent dipole (Cl$^{\delta-}$–Al$^{\delta+}$). In comparison, the **ClAlNPc** molecule with asymmetric planar molecular cyclic structure does not demonstrate appreciable photoexcitation-dependent *C–f* characteristics, confirming the absence of dissociated charge carriers due to the high electron–hole binding energy.

Conclusions

In summary, we have demonstrated the high NIR sensing capability with photocurrent gain of 3×10^5 and EQE of 14% (at zero bias) and 43% (at 3 V) by using four-fold symmetric **ClAlPc** molecules as a single active layer without BHJ structures. Moreover, this single-component (**ClAlPc**) active layer OPD exhibits a record-high linear dynamic range (LDR) of 170 dB with 8 orders of magnitude difference in photocurrent response and submicrosecond response time, which is comparable with the commercial Si-PD. The extraordinary performance of the **ClAlPc**-based OPD device indicates that the electron–hole binding energy must be surprisingly low to effectively dissociate the photogenerated electron–hole pairs, towards direct generation of free carriers under photoexcitation. More importantly, our bias-dependent magneto-photocurrent studies found that introducing the symmetry of charge density to the planar molecular ring provides a fundamental mechanism to significantly lower the electron–hole binding energy in organic molecules known as low-dielectric materials. We observed that the critical bias required to complete the dissociation of photogenerated electron–hole pairs reaches an extremely low value of 24.8 mV in four-fold symmetric **ClAlPc** molecules. This reflects a significantly reduced electron–hole binding energy when introducing the four-fold symmetry of charge density through the molecular design of planar macrocyclic conjugated ring systems. Furthermore, the vertical electric dipole (Cl$^{\delta-}$–Al$^{\delta+}$) can facilitate electron–hole pair dissociation and electrical conduction in four-fold symmetric **ClAlPc** molecules. In contrast, decreasing the symmetry of charge density to three-fold structure, the **SubPc** molecules demonstrate a higher critical bias of 128 mV to complete the dissociation of electron–hole pairs. Furthermore, by breaking the symmetry of charge density, the critical bias required to dissociate the electron–hole pairs is greatly increased to 525 mV in the analogous counterpart **ClAlNPc** with asymmetric molecular ring composed of three planar isoindole rings and one benzoisoindole ring. Clearly, increasing the symmetry of charge density can lead to an extraordinary NIR photosensing capability by using the **ClAlPc** molecules as a single-component active layer based on the device architecture of ITO/**ClAlPc** (10 nm)/TAPC (90 nm)/MoO_3 (15 nm)/Al (120 nm). Fundamentally, our bias-dependent magneto-photocurrent studies indicate that increasing the symmetry of charge density presents an underlying mechanism to significantly lower the electron–hole

binding energies in organic molecules for energy-related optoelectronic applications.

Experimental methods

Materials and device fabrication

The chloroaluminum phthalocyanine (**ClAlPc**), phthalocyanine (Pc), boron subphthalocyanine chloride (**SubPc**), 1,1-bis(di-4-tolyl-aminophenyl)cyclohexane (TAPC), MoO_3 and Al were purchased from Sigma-Aldrich. The asymmetrical **ClAlNPc** was synthesized using the detailed synthesis procedure found in the ESI.† The organic material of **ClAlPc** was sublimated twice by using a homemade purification system according to previously reported procedures. The ITO substrates, with a sheet resistance of approximately 15 Ohm sq^{-1}, were purchased from Luminescence Technology Corporation. For the cleaning process, the sample was cleaned in an ultrasonic bath in successive solutions, dilute detergent, acetone, and isopropanol, and soaked in DI water. Organic thin-film was deposited using a thermal evaporator with a high vacuum of 5×10^{-6} Torr, while the quartz crystal monitor was used to detect the film thickness *in situ*. Note that all fabrication processes were appropriately encapsulated in a nitrogen-filled glove box. For measurement, our device active area of 4 mm^2 was defined by cross-area of anode and cathode pads.

Theoretical calculation

The calculations were accomplished with the Guassian 09 suit of programs through Taiwania. The ground-state geometry optimizations of **ClAlPc** and **ClAlNPc** were conducted in gaseous state at a B3LYP/6-31g(d,p) level utilizing density functional theory (DFT). The S_1 state geometry optimizations of **ClAlPc** and **ClAlNPc** were conducted in gaseous state at a B3LYP/6-31g(d,p) level *via* utilizing time-dependent density functional theory (TD-DFT). All the electrostatic potential surfaces (ESP) were attained after the geometry optimization and mapped at the 0.047 electron density. We are grateful to the National Center for High-Performance Computing for computer time and facilities for the computing resources.

Measurements and characterizations

In the photodetector performance characterizations, the current density–voltage characteristics of NIR OPDs were measured with a source meter (Keithley 2636A) in the dark and under 780 nm illumination (Thorlabs LED780L) at 2 mW cm^{-2}, respectively. The device current gain ratio was defined as the light current density divided by dark current density. To examine the photovoltaic characteristics for single-active-layer devices (ITO/active layer/Al), the devices were measured with a current source meter (Keithley 2401) under dark and under AM 1.5G solar simulator (Newport 91160). Note that the intensity of 1 sun (100 mW cm^{-2}) was calibrated using a Si reference cell (PV measurement; area: 3.981 cm^2). A monochromator (Newport 74100) and lock-in amplifier (Signal Recovery 7265) chopped at 250 Hz were used to evaluate the EQE of our devices. The absorption spectrum of the organic layer was determined using an ultraviolet (UV)-visible spectrophotometer (Thermo Scientific Evolution 220). For linear dynamic range (LDR) measurement, the illumination source was the NIR LED (Thorlabs LED780L) and laser (CNI MLL-III-785) to irradiate the OPDs, while the device photocurrent was recorded using a source meter (Keithley 2636). To adjust the pumping intensity, the optical wheel with ND filter was turned to set the various power densities from 1 W cm^{-2} to 10 pW cm^{-2}, which were calibrated by the precision power meter (Newport power meter Model 1936-R). To estimate the LDR value, we used the equation LDR (dB) = $20\log(J_{ph}/J_{dark})$, where J_{ph} and J_{dark} represent the photocurrent of the device obtained under light (1 W cm^{-2}) and dark (10 pW cm^{-2}) conditions. For the photocurrent response behavior measurement, the LED (Thorlabs LED780L) with a pulse width of 10 kHz was modulated by the function generator (Tektronix AFG3120C) as excitation NIR light source (780 nm). The light intensity was set at 2 mW cm^{-2}. Our proposed photodiode was connected to the 2.5 GHz oscilloscope (LeCroy Waverunner 625Zi) with pre-amplifier (Signal Recovery 5182 Model). The frequency response was recorded with a NIR LED (Thorlabs LED780L) driven by a function generator (Tektronix AFG3120C) to create a pulse waveform with a frequency from 10^2 to 10^6 Hz. The measurement signal used the pre-amplifier (Signal Recovery 5182 Model) connected to a digital oscilloscope (LeCroy Waverunner 625Zi). Then, the raw data were analyzed using fast Fourier transformation to calculate the value of cut-off frequency. The stability test was performed in encapsulated devices at ambient condition with the temperature of 27 °C and the humidity of 60%. The magneto-photocurrent signals were measured by monitoring the photocurrent value (Keithley 2400) as a function of magnetic field at room temperature. The magneto-photocurrent amplitude is defined as: $\mathrm{MFE} = \frac{I_B - I_0}{I_0}$, where I_B and I_0 are the photocurrents with and without an external magnetic field. The photoexcitation was from a 785 nm CW laser. The impedance measurements were carried out using an Agilent E4980A LCR meter under an alternating bias of 50 mV.

Author contributions

M. W. performed the bias-dependent magneto-photocurrent measurements and *C–f* measurements. B. H. supervised the experimental studies. Y.-Z. L. and C.-W. L. prepared and characterized the OPDs, the hole-only devices for the SCLC and the OPVs. H.-C. C. synthesized and characterized the **ClAlNPc** molecule. Y.-S. C. and Y.-C. L. conducted the theoretical analyses of excited-state electrostatic potential maps. C.-S. T. and Y.-C. H. conducted the GIWAXS and GISAXS analyses. M. W., S.-W. L., K.-T. W. and B. H. provided ideas for rationalizing the results and preparing the manuscript.

Conflicts of interest

There are no conflicts to declare.

Acknowledgements

This research was supported by the Air Force Office of Scientific Research (AFOSR) under the grant number FA 9550-15-1-0064, AOARD (FA2386-15-1-4104), and National Science Foundation (NSF-1911659). This research was partially conducted at the Center for Nanophase Materials Sciences based on user projects (CNMS2017-102), which is sponsored by Oak Ridge National Laboratory and the Division of Scientific User Facilities, U.S. Department of Energy. The supports granted from the Ministry of Science and Technology Taiwan (107-2113-M-002-019-MY3, 107-2119-M-131-001, 108-2221-E-131-027-MY2) are also acknowledged.

References

1 H. Tanaka, T. Yasuda, K. Fujita and T. Tsutsui, *Adv. Mater.*, 2006, **18**, 2230–2233.
2 G. Simone, D. Di Carlo Rasi, X. de Vries, G. H. Heintges, S. C. Meskers, R. A. Janssen and G. H. Gelinck, *Adv. Mater.*, 2018, **30**, 1804678.
3 Z. Wu, Y. Zhai, W. Yao, N. Eedugurala, S. Zhang, L. Huang, X. Gu, J. D. Azoulay and T. N. Ng, *Adv. Funct. Mater.*, 2018, **28**, 1805738.
4 S. Park, K. Fukuda, M. Wang, C. Lee, T. Yokota, H. Jin, H. Jinno, H. Kimura, P. Zalar and N. Matsuhisa, *Adv. Mater.*, 2018, **30**, 1802359.
5 J. Clark and G. Lanzani, *Nat. Photonics*, 2010, **4**, 438.
6 E. H. Sargent, *Adv. Mater.*, 2008, **20**, 3958–3964.
7 X. Hu, K. Wang, C. Liu, T. Meng, Y. Dong, S. Liu, F. Huang, X. Gong and Y. Cao, *J. Mater. Chem. C*, 2014, **2**, 9592–9598.
8 L. Zhang, T. Yang, L. Shen, Y. Fang, L. Dang, N. Zhou, X. Guo, Z. Hong, Y. Yang and H. Wu, *Adv. Mater.*, 2015, **27**, 6496–6503.
9 L. Li, Y. Huang, J. Peng, Y. Cao and X. Peng, *J. Mater. Chem. C*, 2014, **2**, 1372–1375.
10 H. Zhang, S. Jenatsch, J. De Jonghe, F. Nüesch, R. Steim, A. C. Véron and R. Hany, *Sci. Rep.*, 2015, **5**, 9439.
11 X. Wang, H. Li, Z. Su, F. Fang, G. Zhang, J. Wang, B. Chu, X. Fang, Z. Wei and B. Li, *Org. Electron.*, 2014, **15**, 2367–2371.
12 Z. Su, F. Hou, X. Wang, Y. Gao, F. Jin, G. Zhang, Y. Li, L. Zhang, B. Chu and W. Li, *ACS Appl. Mater. Interfaces*, 2015, **7**, 2529–2534.
13 M.-S. Choi, S. Chae, H. J. Kim and J.-J. Kim, *ACS Appl. Mater. Interfaces*, 2018, **10**, 25614–25620.
14 S. R. Forrest, *Nature*, 2004, **428**, 911.
15 M. Knupfer, *Appl. Phys. A: Mater. Sci. Process.*, 2003, **77**, 623–626.
16 W. Wang, F. Zhang, M. Du, L. Li, M. Zhang, K. Wang, Y. Wang, B. Hu, Y. Fang and J. Huang, *Nano Lett.*, 2017, **17**, 1995–2002.
17 R. K. Canjeevaram Balasubramanyam, A. E. Kandjani, C. J. Harrison, S. S. A. Abdul Haroon Rashid, Y. M. Sabri, S. K. Bhargava, R. Narayan, P. Basak and S. J. Ippolito, *ACS Appl. Mater. Interfaces*, 2017, **9**, 27875–27882.
18 K. Karimov, S. Moiz, M. M. Tahir, N. Ahmed, R. Tariq, S. Abbas and Q. Zafar, *J. Optoelectron. Adv. Mater.*, 2014, **16**, 1430–1435.
19 X. He, G. Zhu, J. Yang, H. Chang, Q. Meng, H. Zhao, X. Zhou, S. Yue, Z. Wang and J. Shi, *Sci. Rep.*, 2015, **5**, 17076.
20 H. T. Chandran, T. W. Ng, Y. Foo, H. W. Li, J. Qing, X. K. Liu, C. Y. Chan, F. L. Wong, J. A. Zapien and S. W. Tsang, *Adv. Mater.*, 2017, **29**, 1606909.
21 K. Cnops, B. P. Rand, D. Cheyns, B. Verreet, M. A. Empl and P. Heremans, *Nat. Commun.*, 2014, **5**, 3406.
22 S. W. Liu, C. C. Lee, C. H. Yuan, W. C. Su, S. Y. Lin, W. C. Chang, B. Y. Huang, C. F. Lin, Y. Z. Lee and T. H. Su, *Adv. Mater.*, 2015, **27**, 1217–1222.
23 S.-W. Liu, Y.-Z. Li, S.-Y. Lin, Y.-H. Li and C.-C. Lee, *Org. Electron.*, 2016, **30**, 275–280.
24 C.-H. Yuan, C.-C. Lee, C.-F. Liu, Y.-H. Lin, W.-C. Su, S.-Y. Lin, K.-T. Chen, W.-C. Chang, Y.-Z. Li and T.-H. Su, *Sci. Rep.*, 2016, **6**, 32324.
25 J. Miao and F. Zhang, *J. Mater. Chem. C*, 2019, **7**, 1741–1791.
26 W. L. Tsai, C. Y. Chen, Y. T. Wen, L. Yang, Y. L. Cheng and H. W. Lin, *Adv. Mater.*, 2019, **31**, 1900231.
27 H. L. Zhu, Z. Liang, Z. Huo, W. K. Ng, J. Mao, K. S. Wong, W. J. Yin and W. C. Choy, *Adv. Funct. Mater.*, 2018, **28**, 1706068.
28 W. Wang, D. Zhao, F. Zhang, L. Li, M. Du, C. Wang, Y. Yu, Q. Huang, M. Zhang and L. Li, *Adv. Funct. Mater.*, 2017, **27**, 1703953.
29 Y.-H. Tak, K.-B. Kim, H.-G. Park, K.-H. Lee and J.-R. Lee, *Thin Solid Films*, 2002, **411**, 12–16.
30 F. Nüesch, E. Forsythe, Q. Le, Y. Gao and L. Rothberg, *J. Appl. Phys.*, 2000, **87**, 7973–7980.
31 D. Yang and D. Ma, *Adv. Opt. Mater.*, 2019, **7**, 1800522.
32 R. D. Jansen-van Vuuren, A. Armin, A. K. Pandey, P. L. Burn and P. Meredith, *Adv. Mater.*, 2016, **28**, 4766–4802.
33 J. Miao and F. Zhang, *Laser Photonics Rev.*, 2019, **13**, 1800204.
34 P. W. Blom, M. De Jong and J. Vleggaar, *Appl. Phys. Lett.*, 1996, **68**, 3308–3310.
35 C.-F. Lin, S.-W. Liu, C.-C. Lee, J.-C. Hunag, W.-C. Su, T.-L. Chiu, C.-T. Chen and J.-H. Lee, *Sol. Energy Mater. Sol. Cells*, 2012, **103**, 69–75.
36 Z. Xu and B. Hu, *Adv. Funct. Mater.*, 2008, **18**, 2611–2617.
37 A. Schellekens, W. Wagemans, S. Kersten, P. Bobbert and B. Koopmans, *Phys. Rev. B: Condens. Matter Mater. Phys.*, 2011, **84**, 075204.
38 V. Mihailetchi, L. Koster, J. Hummelen and P. Blom, *Phys. Rev. Lett.*, 2004, **93**, 216601.
39 D. Veldman, O. Ipek, S. C. Meskers, J. R. Sweelssen, M. M. Koetse, S. C. Veenstra, J. M. Kroon, S. S. van Bavel, J. Loos and R. A. Janssen, *J. Am. Chem. Soc.*, 2008, **130**, 7721–7735.
40 Y.-C. Hsiao, T. Wu, M. Li, W. Qin, L. Yu and B. Hu, *Nano Energy*, 2016, **26**, 595–602.
41 H. Xu, M. Wang, Z.-G. Yu, K. Wang and B. Hu, *Adv. Phys.*, 2019, **68**, 49–121.